Engineering Structures 33 (2011) 1326–1337

Contents lists available at ScienceDirect

Engineering Structures

journal homepage: www.elsevier.com/locate/engstruct

Climate change impact and risks of concrete infrastructure deterioration

Mark G. Stewart [a,*], Xiaoming Wang [b], Minh N. Nguyen [c]

[a] Centre for Infrastructure Performance and Reliability, The University of Newcastle, New South Wales, 2308, Australia

[b] CSIRO Climate Adaptation Flagship and CSIRO Sustainable Ecosystems, Commonwealth Scientific and Industrial Research Organisation (CSIRO), PO Box 56, Graham Rd., Highett, Victoria 3190, Australia

[c] CSIRO Climate Adaptation Flagship and CSIRO Land and Water, Commonwealth Scientific and Industrial Research Organisation (CSIRO), PO Box 56, Graham Rd., Highett, Victoria 3190, Australia

ARTICLE INFO

Article history:
Received 25 March 2010
Received in revised form
10 January 2011
Accepted 12 January 2011
Available online 8 February 2011

Keywords:
Risk
Structural reliability
Climate change
Corrosion
Concrete

ABSTRACT

Atmospheric CO_2 is a major cause of reinforcement corrosion in bridges, buildings, wharves, and other concrete infrastructure in Australia, United States, United Kingdom and most other countries. The increase in CO_2 levels associated with global warming will increase the likelihood of carbonation-induced corrosion. Moreover, temperature rises will increase corrosion rates. Clearly, the impact of climate change on existing and new infrastructure is considerable, as corrosion damage is disruptive to society and costly to repair. The paper describes a probabilistic and reliability-based approach that predicts the probability of corrosion initiation and damage (severe cracking) for concrete infrastructure subjected to carbonation and chloride-induced corrosion resulting from elevated CO_2 levels and temperatures. The atmospheric CO_2 concentration and local temperature and relative humidity changes with time over the next 100 years in the Australian cities of Sydney and Darwin are projected based on nine General Circulation Models (GCMs) under (i) high CO_2 emission scenario, (ii) medium CO_2 emission scenario, and (iii) CO_2 emission reduction scenario based on policy intervention. The probabilistic analysis included the uncertainty of CO_2 concentration, deterioration processes, material properties, dimensions, and predictive models. It was found that carbonation-induced damage risks can increase by over 400% over a time period to 2100 for some regions in Australia. Damage risks for chloride-induced corrosion increase by no more than 15% over the same time period due to temperature increase, but without consideration of ocean acidity change in marine exposure. Corrosion loss of reinforcement is not significant. The results were most sensitive to increases in atmospheric CO_2.

1. Introduction

Infrastructure is a key component of human settlement that facilitates activities of the population via buildings, transport, energy, water, and communication. For example, following the pattern of population distribution and industrial activities, transport infrastructure has been concentrated near the cities of Melbourne, Sydney and Brisbane and along the south east coast of Australia—this region of Australia has a temperate climate zone. Key ports are distributed more widely around Australia and serve as important export functions for primary resources—some of these ports, including Darwin, lie in a tropical climatic zone. In fact, over $1.1 trillion of Australia's wealth is locked up in homes, commercial buildings, ports and other physical infrastructure assets, which is equivalent to nine times the current national budget or twice the GDP of Australia. Concrete construction is the predominant construction type for most critical infrastructure, and its performance is therefore vital to underpinning the nation's essential services and economic activities. Australia is not unique in this regard, as most countries including the United States, Canada and Europe rely on concrete infrastructure for their social and economic well-being, and face similar climatic characteristics to Australia.

Deterioration is regarded as one of the major factors that could significantly change the long-term performance of concrete structures (e.g., [1–3]). It is well-known that the deterioration rate not only depends on material compositions and construction processes, but also relies on the on-going climatic environment during the service phase of the structures' life cycle. Climate change may alter this environment, especially over longer terms, causing acceleration of the deterioration process, causing corrosion-induced cracking and spalling, which will result in more costly and disruptive repairs, as well as strength loss of concrete structures.

Decisions relating to infrastructure development, maintenance, replacement or refurbishment come with a long-term commitment and can have consequences for periods of 30–200 years or

* Corresponding author. Tel.: +61 2 49216027.
E-mail addresses: mark.stewart@newcastle.edu.au (M.G. Stewart), xiaoming.wang@csiro.au (X. Wang), minh.nguyen@csiro.au (M.N. Nguyen).

0141-0296/$ – see front matter © 2011 Elsevier Ltd. All rights reserved.
doi:10.1016/j.engstruct.2011.01.010

more. These decisions and associated investments will need to take into account future climate conditions. Therefore, efforts in analysis of the implications of climate change impacts will assist us to deal with decision-making for the issues which may emerge in the future, to protect our national infrastructure and human settlements.

The Intergovernmental Panel on Climate Change fourth assessment report [4] indicated a significant increase of CO_2 concentration in the atmosphere from 280 ppm in 1750 to 380 ppm in 2005 with an increasing trend. In comparison with pre-industrial temperatures, the best estimation of the temperature increase from 1990 caused by increasing atmospheric CO_2 concentration can be 2.1 °C for 550 ppm CO_2, 3.0 °C for 700 ppm, and 4.4 °C for 1000 ppm CO_2 by 2100 [4]. Increased temperature will increase rates of carbonation and chloride penetration, as well as corrosion rate. For example, we will see later in the paper that corrosion rates will increase by up to 15% if temperature increases by 2 °C.

Current levels of atmospheric CO_2 of about 380 ppm will, in many cases, not cause significant carbonation-induced corrosion [5]. Sudret et al. [6] developed spatial reliability models to predict the likelihood and extent of corrosion damage induced by carbonation, but this work assumed a constant (time-invariant) CO_2 concentration. When developing reliability-based durability design specifications the fib Model Code for Service Life Design [7] adopted a CO_2 concentration of approximately 500 ppm based on a linear increase of 1.5 ppm/yr over 100 years. However, this work only considered corrosion initiation as the limit state, and the Intergovernmental Panel on Climate Change [4] predicted CO_2 concentrations exceeding 1000 ppm by 2100 for some carbon emission scenarios. Stewart et al. [8] found that the ambient CO_2 concentration attributable to a typical urban environment is approximately 5%–10% higher than CO_2 concentrations in a rural environment. The concentration of CO_2 in urban environments is influenced by combustion of fossil fuels from traffic, domestic heating, power generation, etc., and CO_2 concentrations are often higher, closer to the ground level. Carbonation depths were then calculated for Reinforced Concrete (RC) structures assuming a climate change prediction of up to 450 ppm for service lives of up to 100 years [8]. The probabilistic analysis showed that variability in carbonation depths can be high due to uncertainty and variability of environmental and material properties. Peng and Stewart [9] used the latest CO_2 concentration data provided by the fourth assessment report of 2007 Intergovernmental Panel Climate Change [4] to predict the likelihood and extent of carbonation-induced corrosion and cover cracking and safety loss to RC and prestressed concrete beams in flexure and shear. Stewart and Peng [10] then conducted a life cycle cost assessment to assess the cost-effectiveness of increasing design cover as an adaptation measure to mitigate the effects of carbonation of concrete. The effect of climate change on chloride-induced corrosion appears to have also been the subject of relatively little research. However, Bastidas-Arteaga et al. [11] have calculated 5%–15% increases in probability of corrosion initiation due to climate change. Moreover, El Hassan et al. [12] have highlighted the important effect of changes in climatic conditions on structural reliability.

The paper describes a probabilistic and reliability-based approach that predicts (i) probability of corrosion initiation, (ii) probability of corrosion damage (severe cracking), and (iii) corrosion loss of reinforcement for concrete infrastructure subjected to corrosion resulting from higher CO_2 levels and temperatures. The atmospheric CO_2 concentration and local temperature and humidity changes with time over the next 100 years are projected for the Australian cities of Sydney and Darwin—these cities are representative of temperate and tropical climates, respectively. Many parts of the United States, Canada and Europe have similar temperate or tropical climates. Temperature and humidity projections will be based on nine General Circulation Models (GCMs) under (i) high CO_2 emission scenario, (ii) medium CO_2 emission scenario, and (iii) CO_2 emission reduction scenario based on policy intervention. The reference or 'best' case scenario where CO_2 concentration levels are held constant at year 2000 levels is also considered. Atmospheric CO_2 concentration, temperature and humidity are considered in this paper as three of the major environmental influences on corrosion processes. Two types of corrosion agents of concern are modelled: (i) carbonation and (ii) chloride (marine exposure) induced corrosion. The probabilistic analysis includes the uncertainty of CO_2 concentration, deterioration processes, material properties, dimensions, and predictive models. A computer program named CIRCAA-RC (Climate Impact Risks for Corrosion Adaptation Assessment-Reinforced Concrete) was developed to calculate the climate impact risks for above ground OPC (Ordinary Portland Cement) concrete infrastructure, but it can be extended for other types of concrete.

2. Anthropogenic aspects of climate change

To project the anthropogenic impact due to emissions in relation to population, economy, technology, energy, land use and agriculture, a total of four scenario families, i.e., A1, A2, B1 and B2, are defined [13]. The A1 scenario indicates very rapid economic growth, a global population that peaks in mid-century and declines thereafter, and the rapid introduction of new and more efficient technologies, as well as substantial reduction in regional differences in per capita income. The A2 scenarios represents a very heterogeneous world with preservation of local identities, continuous increase of population, regionally oriented economic development, more fragmented per capita economic growth and technological change. The B1 scenarios assumes the same population trend as A1, but rapid change in economic structures towards a service and information economy, reduction in material intensity, and introduction of clean and resource efficient technologies. The B2 scenarios has emphasis on local solutions to economic, social and environmental sustainability, continuous increase of global population at a rate lower than A2, intermediate levels of economic development and less rapid and more diverse technological change than those in B1 and A1. Sub-categories of A1 scenario include:

- A1FI considers a carbon emission scenario, which assumes very rapid economic growth, a global population that peaks in mid-century and declines thereafter, and the rapid introduction of new and more efficient technologies, substantial reduction in regional differences in per capita income, intensive fossil energy consumption;
- A1B has similar assumptions as A1FI except balanced fossil and non-fossil energy consumption.

In addition, the scenario of CO_2 stabilisation at 550 ppm by the year 2150 is also introduced to consider the effect of policy intervention. Considering the uncertainties in future global carbon emissions, the impact assessment in the current study is carried out using three carbon emission scenarios, i.e. A1FI, A1B and 550 ppm stabilisation scenarios, representing high emissions, medium emissions and the emissions under policy influences, respectively. An emission scenario based on year 2000 CO_2 levels is also considered to provide a reference for other emission scenarios. Fig. 1 describes the projection of CO_2 concentrations from 1990 based on the Model for Assessment of Greenhouse-gas Induced Climate Change, known as MAGICC [14], specifically related to A1FI, A1B and 550 ppm CO_2 stabilisation scenarios. Their low and upper bounds are also described to consider CO_2 projection modelling errors.

To project spatially dependent temperature increases in the future under different emission scenarios, various climate models or Atmosphere-Ocean General Circulation Models (AOGCMs) have

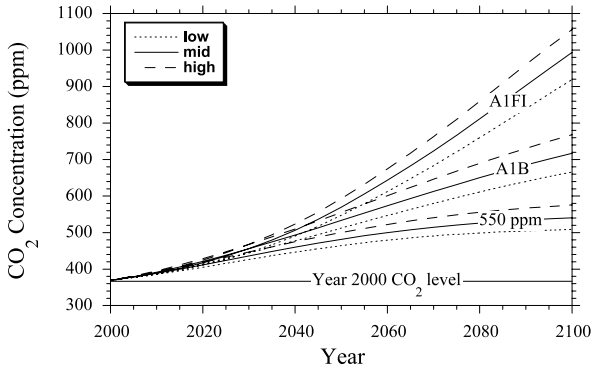

Fig. 1. Predicted low, mid and high estimates of CO_2 concentrations.

been developed based on physical principles at the continental scale. Selecting an AOGCM to be used in an impact assessment is not a trivial task, given the variety of models. The IPCC suggested that due to the varying sets of strengths and weaknesses of various AOGCMs, no single model can be considered the best. Therefore, it is necessary to use multiple models to take into account the uncertainties of models in any impact assessment. In the current study, climate projections from nine climate models are used; for more details see [15,4]. From the global CO_2 concentration and temperature rise projections obtained by MAGICC for a given emission scenario, temperature and relative humidity changes in Australia with different GCMs can be projected by OZClim. OZClim is a climate change projection software developed by the Commonwealth Scientific and Industrial Research Organisation (CSIRO), which is based on the WCRP CMIP3 multimodel dataset developed by the Program for Climate Model Diagnosis and Intercomparison (PCMDI), and the Working Group on Coupled Modelling (WGCM) of World Climate Research Programme (WCRP). For example, Fig. 2 shows the projected median temperatures for each of the nine GCM projections, for A1FI, A1B, 550 ppm and year 2000 emission scenarios for the Australian cities of Sydney and Darwin. Fig. 2 shows that although Darwin has higher temperatures, by 2100 the variability of temperature change is higher for Sydney, for all emission scenarios.

If low and high values shown in Fig. 1 are taken as 10th and 90th percentiles of a normal distribution, respectively, then the statistical parameters for CO_2 concentrations are mean $\mu_{CO_2}(t)$ is equal to mid value, and standard deviation $\sigma_{CO_2}(t)$ is (high–low)/2.56. The Coefficient of Variation (COV) increases with time to a maximum value of approximately 0.06 for all emission scenarios. For the reference (best) emission scenario based on constant year 2000 CO_2 concentration then $\mu_{CO_2}(t) = 369.2$ ppm and $\sigma_{CO_2}(t) = 0$. In all cases the probability distributions are censored at year 2000 CO_2 concentration. The variability of temperature rise and relative humidity change are incorporated through the analysis of nine GCMs.

A number of studies have shown elevated CO_2 levels in urban environments due to higher pollution, exhaust fumes, etc. Stewart et al. [8] recorded CO_2 concentrations of up to 575 ppm in Brno (Czech Republic), with CO_2 concentrations higher near street level. George et al. [16] found that CO_2 concentrations in an urban site (Baltimore) were on average 16% higher than a rural site, and increases of 21%–31% were reported in the literature. Day et al. [17] observed an average enhancement over the course of the day in CO_2 concentration near an urban centre (Phoenix) of 19 ppm. Considering that most infrastructure is located in urban environments, the effects of urban environment on atmospheric CO_2 concentrations should be considered. As most infrastructure is located in urban environments, atmospheric CO_2 concentrations will be increased by a new factor k_{urban}. In this paper, and in the absence of any statistical data on k_{urban}, k_{urban} is assumed normally distributed with mean of 1.15 and COV of 0.10.

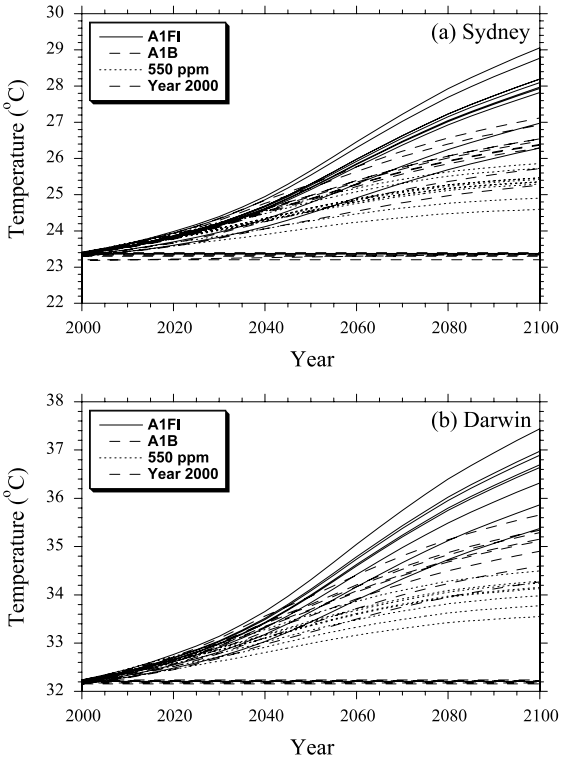

Fig. 2. Projected median temperatures for the nine GCM predictions for the A1FI, A1B, 550 ppm and year 2000 emission scenarios for (a) Sydney and (b) Darwin.

The relative humidity RH(t) is also time-dependent and equal to $\text{RH}(t) = \text{RH}(2000) + \text{RH}_{\text{mid}} \times T_{\text{mid}}(t)$ where $T_{\text{mid}}(t)$ is the median global warming temperature in relation to the emission scenarios and $\text{RH}(t) < 100\%$, and RH_{mid} is the rate of change of relative humidity with the global warming temperature obtained from GCM projections, or the relative humidity change per degree of global warming.

3. Carbonation-induced corrosion

3.1. Time to corrosion initiation

Carbonation depth depends on many parameters: concrete quality, concrete cover, relative humidity, ambient carbon dioxide concentration and others. The impact of carbonation has been studied by many researchers and various mathematical models have been developed with the purpose of predicting carbonation depths (for review see e.g., [18,8]). It is observed that corrosion may occur when the distance between the carbonation front and the reinforcement bar surface is less than 1–5 mm (e.g., [19]). However, probabilistic analyses for assessing durability design specifications tend to ignore this effect [20,7]. Hence, time to corrosion initiation (T_i) occurs when carbonation front equals concrete cover.

The carbonation depth model recommended by DuraCrete [18], Yoon et al. [19] and others considers a wide range of influencing parameters and so the carbonation depth (x_c in cm) is predicted as a diffusion process, but corrected to allow for k_{urban} and t defined in years starting from 2000 as

$$x_c(t) = \sqrt{\frac{2D_{CO_2}(t)}{a} k_{\text{urban}} C_{CO_2}(t - 1999)} \left(\frac{t_o}{t - 1999}\right)^{n_m} \quad t \geq 2000 \tag{1}$$

$$D_{CO_2}(t) = D_1 (t - 1999)^{-n_d} \qquad a = 0.75 C_e C_a O \alpha_H \frac{M_{CO_2}}{M_{CaO}} \tag{2}$$

Table 1
Mean parameter values [19].

w/c	$D_1 \times 10^{-4}$ cm^2 s^{-1}	n_d
0.45	0.65	0.218
0.50	1.24	0.235
0.55	2.22	0.240

Note: for intermediate values use linear interpolation.

where $C_{CO_2}(t)$ is the time-dependent mass concentration of ambient CO_2 (10^{-3} kg/m^3) with $\mu_{CO_2}(t)$ and COV equal to $\sigma_{CO_2}(t)/\mu_{CO_2}(t)$ obtained from Fig. 1 (using the conversion factor 1 ppm $= 0.0019 \times 10^{-3}$ kg/m^3); k_{urban} is a factor to account for increased CO_2 levels in urban environments; $D_{CO_2}(t)$ is the CO_2 diffusion coefficient in concrete; D_1 is CO_2 diffusion coefficient after one year; n_d is the age factor for the CO_2 diffusion coefficient; t_0 is one year; C_e is the cement content (kg/m^3); CaO is the CaO content in cement (0.65); α_H is the degree of hydration; M_{CaO} is the molar mass of CaO (56 g/mol) and M_{CO_2} is the molar mass of CO_2 (44 g/mol). The age factor for microclimatic conditions (n_m) associated with the frequency of wetting and drying cycles is $n_m = 0$ for sheltered outdoor and $n_m = 0.12$ for unsheltered outdoor.

The mean values for D_1 and n_d are given in Table 1, and Yoon et al. [19] provided estimates of maximum (95th percentile) values for D_1 and n_d. The standard deviation for D_1 is approximately 0.15, and COV for n_d is approximately 0.12 for all w/c ratios. These statistics represent model error (or accuracy). The diffusion coefficient D_1 is less than 5×10^{-4} cm^2 s^{-1} which is appropriate for good quality concrete [21]. These parameters are based on $T = 20$ °C and RH = 65%. The degree of hydration for Ordinary Portland Cement (OPC) after more than 400 days is estimated as [22]:

$$\alpha_H \approx 1 - e^{-3.38 w/c}. \tag{3}$$

A higher temperature will cause an increase in diffusion coefficient leading to increased carbonation depths (e.g., [23]). The effect of temperature on diffusion coefficient is modelled using the Arrhenius Law (e.g., [24,19]), where the time-dependent change in diffusion coefficient when compared to a temperature of 20 °C is:

$$f_T(t) \approx e^{\frac{E}{R}\left(\frac{1}{293} - \frac{1}{273+T_{av}(t)}\right)} \quad \text{and} \quad T_{av}(t) = \frac{\sum_{i=2000}^{t} T(t)}{t - 1999} \tag{4}$$

where $T(t)$ is the temperature (°C) at time t, E is the activation energy of the diffusion process (40 kJ/mol [25]) and R is the gas constant (8.314×10^{-3} kJ/mol K). As temperature will be increasing over time, $D_{CO_2}(t)$ is averaged over time and so $T(t)$ is also averaged over time. A 2 °C temperature increase will increase the diffusion coefficient by 12%.

While Eq. (1) was used by Yoon et al. [19] to predict carbonation depths for increases in CO_2 concentrations it needs to be recognised that Eq. (1) is a point-in-time predictive model—i.e., the carbonation depth at time t assumes that $CO_2(t)$ is constant for all times up to time t. This will overestimate carbonation depth as CO_2 concentration will be gradually increasing with time up to the peak value $CO_2(t)$. Stewart et al. [8] considered this phenomenon and calculated carbonation depths due to enhanced atmospheric CO_2 concentration conditions using the average CO_2 concentration over the time period, and not the peak value at time t. As such, Eq. (1) can be re-written as:

$$x_c(t) \approx \sqrt{\frac{2 f_T(t) D_{CO_2}(t)}{a} k_{urban} \int_{2000}^{t} C_{CO_2}(t)\,dt} \times \left(\frac{1}{t - 1999}\right)^{n_m} \quad t \geq 2000. \tag{5}$$

To be sure, Eq. (5) is an approximation, and there is a need for an improved carbonation model that considers the time-dependent effect of CO_2 concentration and other parameters such as temperature or humidity.

Carbonation tends to be highest for relative humidities RH(t) of 50%–70% [26]. Moreover, Al-Khaiat and Fattuhi [27] report that little or no carbonation occurs below a relative humidity of 30%, whereas Russell et al. [26] state that below 50% relative humidity there is insufficient moisture for carbonation reactions to take place. Most carbonation models assume relative humidity of greater than 50%. Some carbonation models explicitly include RH(t) as an influencing parameter (e.g., [18,28]). To be conservative, the analysis assumes that if RH(t) is less than 40% then the carbonation front ceases to advance (i.e. carbonation depth does not increase with time).

3.2. Corrosion propagation

The carbonation-induced corrosion rate is variable and highly dependent on exposure conditions and atmospheric situations; see [29,9] for a review of corrosion rates and models. Some empirical models exist, but each isolates only several variables.

It is interesting to note that when water or oxygen is limited, the corrosion process may eventually stop. In fact, very high humidity in concrete may reduce oxygen diffusion to the corrosion area and slow the corrosion process of reinforcement, while the shortage of water in dry concrete also reduces corrosion activities. The corrosion rate for carbonation or chlorides becomes negligible when relative humidity RH(t) is less than 50% (e.g., [30,31]), and in this study a negligible corrosion rate is defined as a corrosion current density (i_{corr}) of 0.1 μA/cm^2 where a corrosion rate (i_{corr}) of 1 μA/cm^2 = 0.0116 mm/year. The optimum relative humidity for corrosion is 70%–80% [31].

In the present study, corrosion rate is assumed lognormally distributed with statistical parameters for a temperature of 20 °C given by DuraCrete [18]; see Table 2. These values take into account the concrete grades suggested for the corresponding exposure classes. An increase in temperature will increase corrosion rate, and the model described by DuraCrete [24,20] is used:

$$i_{corr}(t) = i_{corr\text{-}20}\,[1 + K(T(t) - 20)] \tag{6}$$

where $i_{corr\text{-}20}$ is the corrosion rate at 20 °C given in Table 2, and $K = 0.025$ if $T(t) < 20$ °C and $K = 0.073$ if $T(t) > 20$ °C. DuraCrete [24,20] notes that Eq. (6) is a close correlation to the Arrhenius equation, at least for temperatures below 20 °C, but may be conservative for $T(t) > 20$ °C. A 2 °C temperature increase will increase the corrosion rate by 15%.

Table 2
Carbonation corrosion rates ($i_{corr\text{-}20}$) for various exposures [18].

Exposure class	Mean	Standard deviation	Distribution
Carbonation			
C1—Dry	0.0[a]	0.0	Lognormal
C2—Wet-rarely dry (unsheltered)	0.345 μA/cm^2	0.259 μA/cm^2	Lognormal
C3—Moderate humidity (sheltered)	0.172 μA/cm^2	0.086 μA/cm^2	Lognormal
C4—Cyclic wet-dry (unsheltered)	0.431 μA/cm^2	0.259 μA/cm^2	Lognormal

[a] Assume negligible = 0.1 μA/cm^2.

Table 3
Surface chloride concentration [34].

Environment	Mean (kg/m^3)	COV	Distribution
C_o1—Splash/tidal zone	7.35	0.7	Lognormal
C_o2—Atmospheric zone on the coast	2.95	0.7	Lognormal
C_o3—Atmospheric zone >1 km from the coast	1.15	0.5	Lognormal

There is little data on time-dependent effects on corrosion rate for carbonated RC structures. Hence, the present analysis assumes a time-invariant corrosion rate for carbonation. This is likely to be a conservative assumption as corrosion rate will generally decrease with time due to the build up of rust products thus impeding the corrosion process (e.g., [32]).

4. Chloride-induced corrosion

4.1. Chloride penetration model

The penetration of chlorides is given empirically by Fick's second law of diffusion. However, chloride penetration processes and field conditions differ from that assumed with Fick's law; for a review see [33]. Nonetheless, Fick's law is often used to describe chloride penetration into concrete due to its computational convenience; namely, surface chloride concentration (C_o) and diffusion coefficients (D_c) are easily calculated by fitting Fick's law to measured chloride profiles. An improved model utilising a time-dependent chloride diffusion coefficient proposed by DuraCrete [24] is used to calculate chloride concentration. Time to corrosion initiation (T_i) is the time at which the chloride concentration at the level of reinforcement exceeds the critical chloride concentration (C_{cr}). The chloride concentration at depth x mm at time t is:

$$C(x,t) = C_o\left[1 - \mathrm{erf}\left(\frac{x}{2\sqrt{k_e \cdot k_t \cdot k_c \cdot f_T(t) D_c \left(\frac{t_o}{t-1999}\right)^n \cdot (t-1999)}}\right)\right] \quad t \geq 2000 \tag{7}$$

where D_c is the apparent chloride diffusion coefficient, n is the ageing factor, k_e is the environment factor, k_t is the test method factor (1.0), k_c is the curing factor (1.0), t_o is the reference time in years (28 days or 0.0767 years), and $f_T(t)$ is the temperature effect on diffusion coefficient given by Eq. (4).

The surface chloride concentration (C_o) is generally assumed as a time-invariant variable as exposure to chlorides for a specific structural member would not change from year to year. However, climate change may cause changes in wetting/drying cycles, rainfall and wind patterns could vary, etc. but there is no data to support how this might affect C_o. The surface chloride concentration can be categorised into specific exposure categories: submerged zone, splash and tidal zones, and atmospheric zone. Surface chloride concentrations for offshore and onshore RC structures in Australia are given in Table 3. The critical chloride concentration is normally distributed with mean and COV of 3.35 kg/m^3 and 0.375, respectively, truncated at 0.35 kg/m^3 [34]. The critical chloride concentration is not affected by concrete quality [24].

There is evidence to suggest that chloride action is accelerated by carbonation (and SO_2, NO_x) because carbonation disturbs the equilibrium between free and bound chlorides in the concrete, thereby increasing the free chloride concentration in the pore solution. However, it appears that this evidence has not been translated into any useful quantitative models. Thus the interaction effect between carbonation and chlorides is, for the time being, omitted from the present study.

4.2. Corrosion propagation

Corrosion rates are highly variable and dependent on concrete grade, cover and environment. For example, the British Standard BS 6349-1 [35] suggests that mean corrosion rate for the atmospheric zone is 0.04 mm/yr (3.45 μA/cm^2), 0.08 mm/yr (6.9 μA/cm^2) for the splash zone, and 0.04 mm/yr (3.45 μA/cm^2) for the tidal zone. The corrosion rates recommended by DuraCrete [18] shown in Table 4 are not dissimilar from those reported in BS 6349-1 [35]. These values take into account the concrete grades suggested for the corresponding exposure classes. Since corrosion rate data given in Table 4 assumes a time-invariant corrosion rate, this analysis will also assume a time-invariant corrosion rate. This is a conservative assumption. The effect of temperature on corrosion rate is modelled using Eq. (6).

5. Time to corrosion damage

Corrosion-induced cover cracking and damage occurs on the concrete surface above and parallel to the rebars. The various stages of crack growth can be described in three stages:

(i) Corrosion initiation (T_i);
(ii) Crack initiation (T_{1st}, time to first cracking—hairline crack of 0.05 mm width), and;
(iii) Crack propagation (T_{sev}, time for crack to develop from crack initiation to a limit crack width, w).

The time to corrosion damage (severe cracking or spalling) is thus $T_{sp} = T_i + T_{1st} + T_{sev}$.

5.1. Time to crack initiation

As there is a porous zone around the steel reinforcing bar the corrosion products must firstly fill this porous zone before the products start to induce internal pressure on the surrounding concrete. Therefore, not all corrosion products contribute to the expansive pressure on the concrete. This approach to crack initiation has been used by El Maaddawy and Soudki [36] and their model is used herein. The thickness of the porous zone (δ_0) is typically in the range of 10–20 μm and can be described using a normal distribution with mean equal to 15 μm and COV of 0.1. It should be noted that the accuracy of the time to severe cracking is

Table 4
Chloride-induced corrosion rates ($i_{corr\text{-}20}$) for various exposures [18].

Exposure class	Mean	Standard deviation	Distribution
Chloride initiated corrosion			
Cl1—Wet-rarely dry	0.345 μA/cm^2	0.259 μA/cm^2	Lognormal
Cl2—Cyclic wet-dry	2.586 μA/cm^2	1.724 μA/cm^2	Lognormal
Cl3—Airborne sea water	2.586 μA/cm^2	1.724 μA/cm^2	Lognormal
Cl4—Submerged	Not expected except bad concrete or lower cover	–	Lognormal
Cl5—Tidal Zone	6.035 μA/cm^2	3.448 μA/cm^2	Lognormal

dominated by the accuracy of time to corrosion initiation (T_i) and the time since crack initiation to reach a limit crack width (T_{sev}), and so service life predictions are relatively insensitive to the crack initiation model [2].

5.2. Time to severe cracking

The time to severe cracking referred to herein is the time when concrete cover cracking reaches a limit crack width of 1 mm. Mullard and Stewart [37] have modelled the rate of crack propagation which enables the time for a crack to develop from crack initiation to a limit crack width (T_{sev}). The time (after crack initiation) for cracking of the concrete surface to reach a crack width of w mm is:

$$T_{sev} = k_R \frac{w - 0.05}{k_c \mathrm{ME}(r_{crack}) r_{crack}} \left(\frac{0.0114}{i_{corr\text{-}20}}\right)$$
$$0.25 \le k_R \le 1,\ k_c \ge 1.0,\ w \le 1.0\ \text{mm} \quad (8)$$

where

$$\psi_{cp} = \frac{\text{Cover}}{Df_t} \quad (9)$$

$$r_{crack} = 0.0008 e^{-1.7\psi_{cp}} \quad 0.1 \le \psi_{cp} \le 1.0 \quad (10)$$

$$k_R \approx 0.95 \left[\exp\left(-\frac{0.3 i_{corr(exp)}}{i_{corr-20}}\right) - \frac{i_{corr(exp)}}{2500 i_{corr-20}} + 0.3\right] \quad (11)$$

and where $i_{corr\text{-}20}$ is the corrosion current density ($\mu A/cm^2$) at $T = 20\ ^\circ C$ and constant with time, ψ_{cp} is the cover cracking parameter, r_{crack} is the rate of crack propagation in mm/h, $\mathrm{ME}_{r_{crack}}$ is the crack propagation model error, w is the crack width (mm), concrete cover is in mm, D is the reinforcing bar diameter in mm, f_t is the concrete tensile strength in MPa, k_R is the rate of loading correction factor where $i_{corr(exp)} = 100\ \mu A/cm^2$ is the accelerated corrosion rate used to derive r_{crack}, and k_c is the confinement factor that represents an increase in crack propagation due to the lack of concrete confinement around external reinforcing bars.

If the reinforcing bar is in an internal location then $k_c = 1$, but for rebars located at edges and corners of RC structures, k_c is in the range 1.2–1.4. Although the data is limited, there appears to be a trend where k_c increases as ψ_{cp} increases. In this study k_c is taken as 1.0. A statistical analysis of model accuracy to account for variabilities between model prediction and experimental data is essential for stochastic or reliability analyses where statistics for model error are required. Hence, the statistics for model error for r_{crack} ($\mathrm{ME}_{r_{rcrack}}$) are: mean($\mathrm{ME}_{r_{crack}}$) = 1.04 and COV($\mathrm{ME}_{r_{crack}}$) = 0.09 [37]. For more details of this improved cover cracking model, see [37]. The cover cracking model developed by Mullard and Stewart [37] was based on chloride-induced corrosion.

Concrete strength is time-variant, and the time-dependent increase in concrete compressive strength after one year using the ACI method is [38] $f_c = 1.162 f_c(28)$ where $f_c(28)$ is the 28 day compressive strength. Time-dependent gains in strength beyond one year are not considered in the present analysis.

5.3. Time to corrosion damage

Since corrosion rate is a time-dependent function of temperature, the time to corrosion damage needs to be corrected since Eqs. (8)–(11) assume a time-invariant (constant) corrosion rate. If we assume that the number of corrosion products needed to cause cracking (m_{corr}) for a constant corrosion rate is directly proportional to $i_{corr}(T_{1st} + T_{sev})$, then $m_{corr} = i_{corr}(T_{1st} + T_{sev})$. The time to corrosion damage for a variable corrosion rate (T_{sp}) is such that the corrosion amounts (m_{corr}) for constant and variable corrosion rates are equal. It follows that T_{sp} is obtained from solving the unknown T_{sp} from the following equation:

$$m_{corr} = \int_{T_i}^{T_{sp}} i_{corr}(t)\mathrm{d}t \quad (12)$$

where $i_{corr}(t)$ is given by Eq. (6).

6. Time-dependent reliability analysis

6.1. Carbonation depth

By using Eq. (5), the percentage increase in carbonation depth when compared to a reference (baseline case) is Eq. (13) which is given in Box I.

Thus, the percentage change in carbonation depth is influenced only by climate variables $f_T(t)$ and $C_{CO_2}(t)$, and not by material related parameters or errors in the carbonation depth model.

6.2. Corrosion initiation

Corrosion will take place when:

1. The carbonation depth reaches the surface of the reinforcing bar, and so the cumulative probability of corrosion initiation at time t is
$$p_i(t) = \Pr[\text{Cover} - x_c(t) < 0] \quad (14)$$
where $x_c(t)$ is the carbonation depth obtained from Eq. (5).
2. The chloride concentration at the level of reinforcement exceeds critical chloride concentration at time t.
$$p_i(t) = \Pr[C_r - C(\text{Cover}, t) < 0] \quad (15)$$
where $C(\text{Cover}, t)$ is the chloride concentration at depth of reinforcement given by Eq. (7), and C_r is the critical chloride concentration.

6.3. Corrosion damage

Corrosion damage is defined as the time when concrete cover severely cracks (crack width $w = 1.0$ mm). Therefore, the cumulative probability of corrosion damage at time t is

$$p_s(t) = \Pr\left[t \ge T_{sp}\right]. \quad (16)$$

If the material, dimensional and corrosion parameters are assumed homogeneous for the structure (i.e. spatial variability is ignored), then the mean proportion of corrosion damage is $p_s(t) \times 100\%$ [6].

6.4. Corrosion loss

Time-dependent corrosion loss of reinforcement is defined as the loss of steel section (reduction in diameter in mm) which is calculated as

$$\Delta d(t) = 2 \times 0.0116 \int_{T_i}^{t} i_{corr}(t)\mathrm{d}t \quad (17)$$

where $i_{corr}(t)$ is given by Eq. (6).

6.5. Computational method

Monte Carlo simulation is used as a computational method for the time-dependent reliability analysis. Note that the CO_2 concentration is fully correlated with time.

Spatial effects for geometric and physical parameters known to influence structural reliabilities are not considered for general

$$P_c(t) = \left[\left(\frac{\sqrt{\frac{2f_T(t)D_{CO_2}(t)}{a}\int_{2000}^{t} C_{CO_2}(t)\mathrm{d}t}\left(\frac{1}{t-1999}\right)^{n_m}}{\sqrt{\frac{2f_T(t=2000)D_{CO_2}(t)}{a}C_{CO_2}(2000)\,(t-1999)}\left(\frac{1}{t-1999}\right)^{n_m}}\right)-1\right]\times 100\%$$

$$= \left[\left(\frac{\sqrt{f_T(t)\int_{2000}^{t} C_{CO_2}(t)\mathrm{d}t}}{\sqrt{f_T(t=2000)C_{CO_2}(2000)\,(t-1999)}}\right)-1\right]\times 100\% \quad (13)$$

Box I.

Table 5
Durability design specifications (AS3600-2009) [40] and deterioration models, for carbonation.

Exposure	Classification	Cover (mm)	F'_c (MPa)	w/c[d] ratio	C_e[a] (kg/m^3)	Mean D_1	Mean n_d	k_{urban}	Sheltered	
									n_m	i_{corr}[e]
Members in exterior environments:										
Inland (>50 km from coast):										
Non-industrial and arid climate	A1	20	20	0.56	320	2.22	0.240	1.15	0.0	C1
Non-industrial and temperate climate	A2	30	25	0.56	320	2.22	0.240	1.15	0.0	C3
Non-industrial and tropical climate	B1	40	32	0.50	320	1.24	0.235	1.15	0.0	C3
Non-industrial and any climate	B1	40	32	0.50	320	1.24	0.235	1.15	0.0	C3
Near-coastal (1–50 km), any climate	B1	40	32	0.50	320	1.24	0.235	1.15	0.0	C3
Coastal (up to 1 km, excluding tidal and splash zones), any climate	B2	45	40	0.46	370	0.65	0.218	1.15	0.0	C3
Surfaces of members in water:										
In tidal or splash zone	C[f]	50	50	0.40	420	0.47[b]	0.19[c]	1.15	0.0	C3

Notes.
[a] Based on minimum cement content specified in AS 5100.5.
[b] Conservative value—highest value based on polynomial, exponential and power extrapolations from Table 1.
[c] Conservative value—lowest value based on polynomial, exponential and power extrapolations from Table 1.
[d] Based on maximum w/c ratio specified in AS 5100.5.
[e] See Table 2.
[f] AS3600-2001.

corrosion as their inclusion will be less important as it is for chloride-induced pitting corrosion (e.g., [39]). However, the inclusion of spatial variability of the environment, dimensions and material properties is an area for further research. For carbonation-induced corrosion it has been shown by Peng and Stewart [9] that enhanced atmospheric CO_2 concentrations have negligible effect on structural reliability for flexure and shear limit states.

7. Results

7.1. Structural configurations

Environmental exposure in Australia is classified by the Australian Concrete Structures Code AS3600-2009 [40] as three climatic zones (arid, temperate and tropical); see Fig. 3. The selected sites of Sydney and Darwin represent two very different macroclimatic conditions for exposed structures, particularly when characterising predicted temperature changes, namely, temperate and tropical climates, respectively. The microclimate, on the other hand, concerns local conditions such as 'aboveground', 'in-ground' and 'maritime' or, more specifically, the position of structural elements in relation to the fluctuating water level (and the time such elements remain dry) and the level of sulphates, pH, and chlorides in the water or soil.

Concrete inside buildings with low air humidity, or that is permanently submerged in water, generally has a low exposure to carbonation, while concrete surfaces subject to long-term periodic water contact, concrete inside buildings with moderate-to-high air humidity, and external concrete sheltered from rain have high exposures to carbonation. In maritime conditions, structures exposed to splash and tide have a significantly higher risk of corrosion than structures that are exposed to airborne salt but are not in direct contact with sea water, or those that are permanently submerged. For these reasons the reliability analyses to follow will focus on corrosion predictions for sheltered and exposed structures for carbonation and chlorides, respectively.

The durability design requirements specified in AS3600 relate to minimum concrete cover and concrete compressive strength, and assumes standard formwork and compaction. Tables 5 and 6 show the durability design specifications related to the AS3600 exposure classifications A1 to C for carbonation and B1 to C2 for chlorides. These tables also show parameter values for the deterioration models, and Table 7 shows the statistical parameters for corrosion parameters, material properties and dimensions—these are representative of concrete structures in Australia. Clearly, the uncertainty and variability of deterioration parameters is considerable. However, improved deterioration modelling may reduce this variability, as could Bayesian updating based on conditions or other site specific data for existing or new structures (e.g., [44–46]). The exposure classifications of most relevance for concrete infrastructure in Sydney and Darwin are near-coastal (B1) and coastal excluding tidal and splash zones (B2). For marine infrastructure, the relevant exposure classifications are C, C1 and C2. However, analyses will be conducted for all exposure classifications to help illustrate the effect of the environment on corrosion damage risks. Unless noted otherwise, all results in the following sections refer to the average of nine GCM temperature simulations. Reinforcement bar diameter is 20 mm.

Note that the 2001 and earlier editions of the Australian Concrete Code AS3600 had a single exposure classification for members in water (exposure classification C). However, the revised (2009) edition now provides more guidance by removing exposure classification C and replacing it with more specific exposure classifications C1 and C2. As nearly all existing infrastructure is designed to AS3600-2001 or earlier then it is important to include exposure classification C in the reliability analyses.

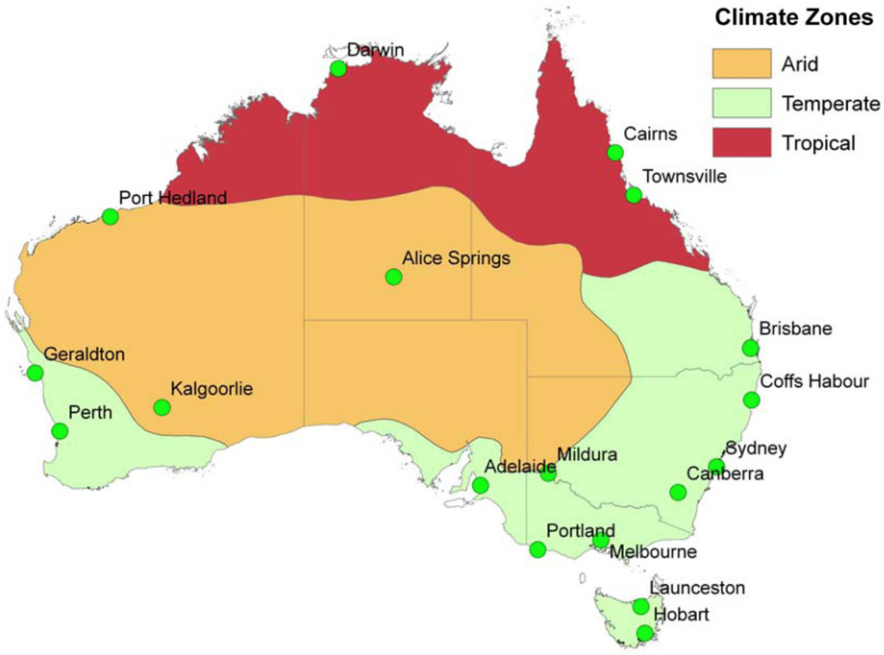

Fig. 3. Climatic zones defined by the Australian concrete code AS3600.

Table 6
Durability design specifications (AS3600-2009) [40] and deterioration models, for chloride-induced corrosion.

Exposure	Classification	Cover (mm)	F'_c (MPa)	w/c[b] ratio	Mean $(D_c) \times 10^{-12}$	Mean (n)	k_e	C_o[c]	i_{corr}[d]
Members in exterior environments:									
Near-coastal (1–50 km), any climate	B1	40	32	0.50	15	0.65	0.676 $\sigma = 0.114$	C_o3	Cl3
Coastal (up to 1 km, excluding tidal and splash zones), any climate	B2	45	40	0.46	10	0.65	0.676 $\sigma = 0.114$	C_o2	Cl3
Surfaces of members in water:									
Splash and tidal zones	C[e]	50	50	0.40	7	0.37	0.924 $\sigma = 0.155$	C_o1	Cl5
In spray zone (>1 m above wave crest level)	C1	50	50	0.40	7	0.37	0.265 $\sigma = 0.045$	C_o2	Cl3
Splash and tidal zones	C2	65	50	0.40	7	0.37	0.924 $\sigma = 0.155$	C_o1	Cl5

Notes
[a] Based on minimum cement content specified in AS 5100.5.
[b] Based on maximum w/c ratio specified in AS 5100.5.
[c] See Table 3.
[d] See Table 4.
[e] AS3600-2001.

The impact assessment is focused primarily on the relative change in corrosion initiation and damage risks due to enhanced CO_2 levels, temperature and humidity when compared to year 2000 levels, and not on the absolute estimates of risk. The deterioration models are mostly derived from the 1996–1999 European DuraCrete project which has formed the basis for the probabilistic durability design of many important structures and the fib Model Code for Service Life Design [7]. However, many other deterioration models have been developed for concrete durability, which if deemed more appropriate, can readily be incorporated into the stochastic and reliability framework developed in the present paper. While different deterioration models will produce different estimates of absolute risk, deterioration model selection will have significantly less influence on comparative risks.

7.2. Carbonation

Fig. 4 shows the mean carbonation depth for the four emission scenarios and five exposure classifications, for Sydney and Darwin. The carbonation depths are higher for Darwin due to the 8 °C increase in temperature when compared to Sydney. The Australian Concrete Structures Code AS3600-2009 [40] specifies improved concrete compressive strength and other enhanced durability design specifications, which will result in a reduced rate of carbonation. This is evident in Fig. 4 where exposure classification C with $w/c = 0.40$ concrete has a carbonation depth significantly less than exposure classification A1 and A2 with $w/c = 0.56$. The A1FI, A1B and 550 ppm emission scenarios have a significant effect on carbonation depths, but the carbonation depths for these

Table 7
Statistical parameters for corrosion parameters, material properties and dimensions.

Parameters	Mean	COV	Distribution	Reference
$f_c(28)$	$1.03F_c'$	0.18	Normal	Pham [41]
D_1	Table 5	$\sigma = 0.15$	Normal	
n_d	Table 5	0.12	Normal	
Age factor (n)	Table 6	$\sigma = 0.07$	Normal	DuraCrete [24]
Environmental factor (k_e)	Table 6	Table 8	Normal	DuraCrete [24]
Diffusion coefficient (D_c)	Table 6	0.285	Normal	DuraCrete [24]
ME(r_{crack})	1.04	0.09	Normal	Mullard and Stewart [37]
k_{urban}	1.15	0.10	Normal[b]	–
Cover[d]	$C_{nom} + 6$ mm	$\sigma = 11.5$ mm	Normal[c]	McGee [42]
f_t	$0.53(f_c)^{0.5}$	0.13	Normal	Mirza et al. [43]
E_c	$4600(f_c)^{0.5}$	0.12	Normal	Mirza et al. [43]

Notes.
[b] Truncated at 1.0.
[c] Truncated at 10 mm (stirrup diameter).
[d] Cover-meter data obtained from 83 RC bridges in Tasmania.

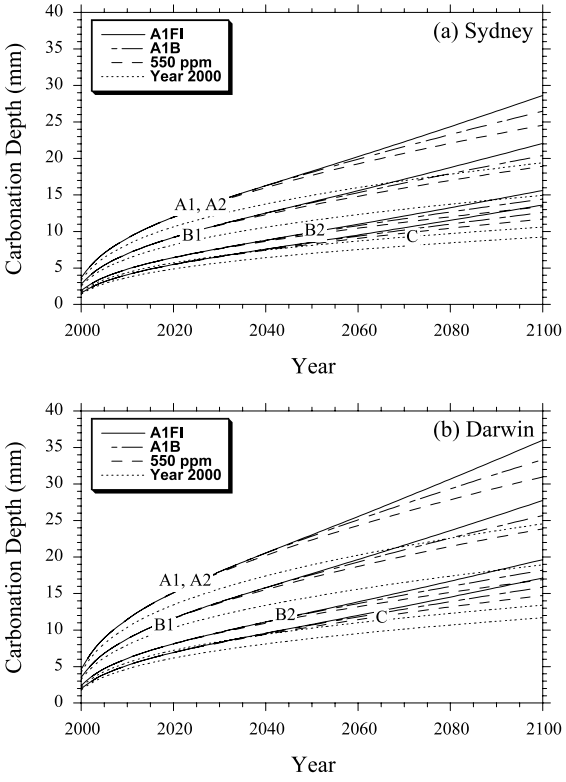

Fig. 4. Mean carbonation depths for (a) Sydney and (b) Darwin.

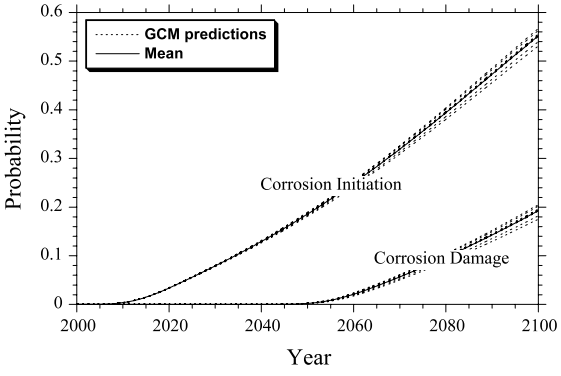

Fig. 5. Effect of nine GCM temperature predictions on probabilities of corrosion initiation and corrosion damage, for Sydney, A1 exposure classification and A1FI emission scenario.

emission scenarios vary by no more than 4 mm by 2100. For example, the A1FI emission scenario increases carbonation depth by approximately 36% when compared to reference year 2000 CO_2 emissions, whereas the 550 ppm by 2150 emission scenario increases carbonation depths by only 25%. Note, that as discussed in Section 6.1, the percentage change in carbonation depth is not influenced by material related parameters.

The effect of the nine GCM temperature prediction models on probabilities of corrosion initiation and corrosion damage are shown in Fig. 5, for A1FI emission scenario and A1 exposure classification in Sydney. There are 6.8% and 17.1% differences between maximum and minimum predicted probabilities of corrosion initiation and damage, respectively. This represents quite low variability, hence, it is reasonable to only consider the average of nine GCM temperature simulations when presenting results.

The probabilities of corrosion initiation and damage are shown in Fig. 6 for all emission scenarios, exposure classifications and locations. The likelihood of corrosion initiation is less than 0.004, and less than 0.002 for corrosion damage, for exposure classifications B2 and C. These probabilities are negligible irrespective of the emission scenario. Corrosion initiation and corrosion damage risks are highest for exposure classifications A1, A2 and B1 as these are exposures most susceptible to carbonation, whereas the other exposure classifications are more related to coastal exposure to chlorides. There is unlikely to be any significant corrosion damage for the first 20–30 years service life, but the likelihood of corrosion damage then increases to 20%–40% for A1FI, A1B and 550 ppm emission scenarios. In practical terms, this is equivalent (see Section 6.1) to expecting that 20%–40% of every concrete surface by the year 2100 will be damaged and in need of maintenance or repair. The probability of corrosion damage for the worst case scenario (A1FI) is up to 460% higher than that observed for the reference (best) mitigation scenario; see Fig. 7. This indicates that the higher CO_2 concentration could lead to a significant likelihood and extent of corrosion damage that may need costly and disruptive repairs during the service life of many concrete structures. A larger bar diameter will result in a corresponding higher likelihood of corrosion damage.

The corrosion loss of reinforcement diameter $\Delta d(t)$ is quite modest due to the long time taken for corrosion initiation and relatively low corrosion rates associated with carbonation. For example, the mean additional corrosion loss (when compared to corrosion loss for the reference mitigation scenario) is 0.23 and 0.08 mm at year 2100 for A1FI emission scenario and exposure A2 for Darwin and Sydney, respectively. These are the highest corrosion loss for any exposure. For a 16 mm diameter bar this represents a 2.8% and 1.0% loss of cross-sectional area, and by inference of structural capacity. For other exposure classifications,

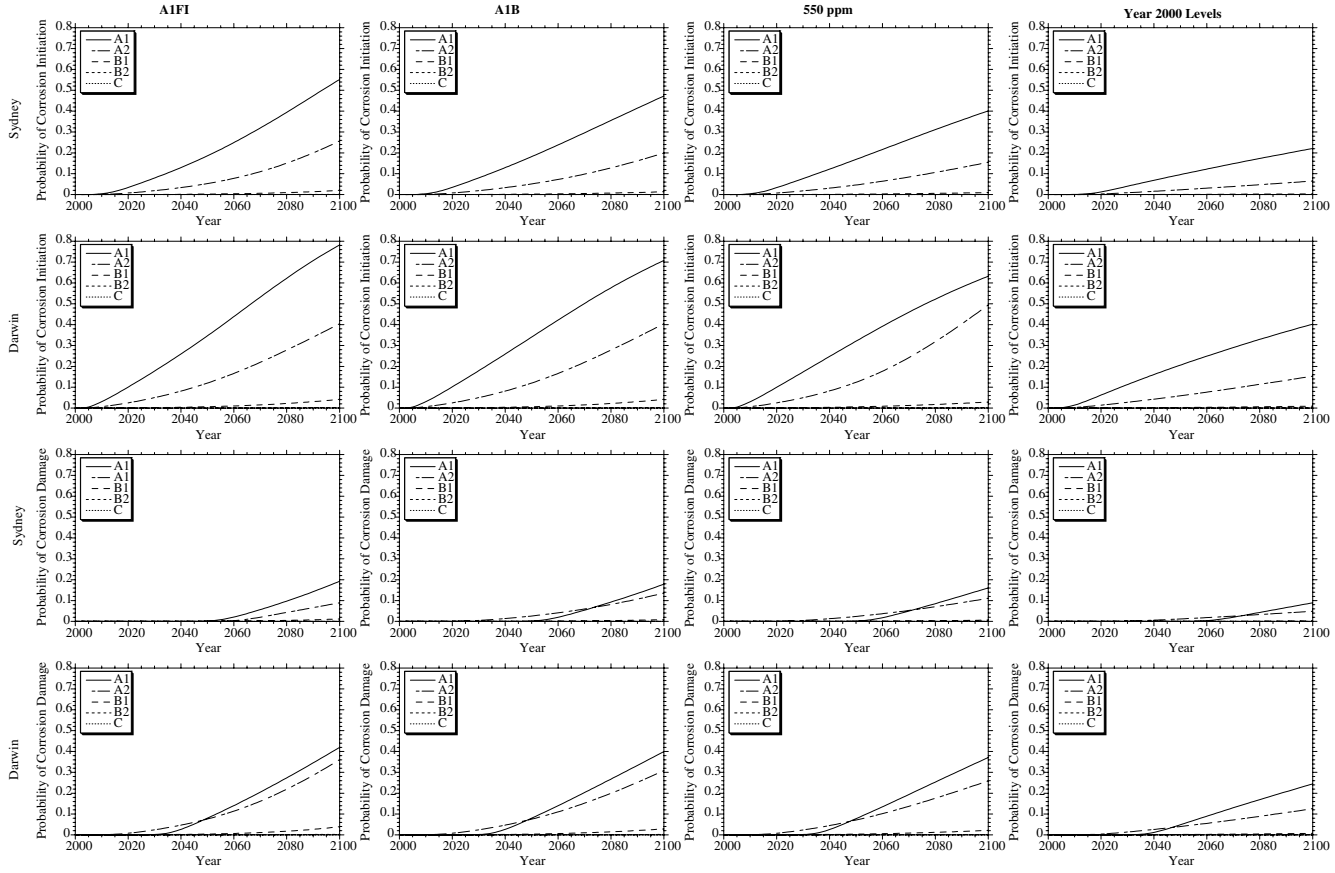

Fig. 6. Probabilities of carbonation-induced corrosion initiation and corrosion damage, for Sydney and Darwin.

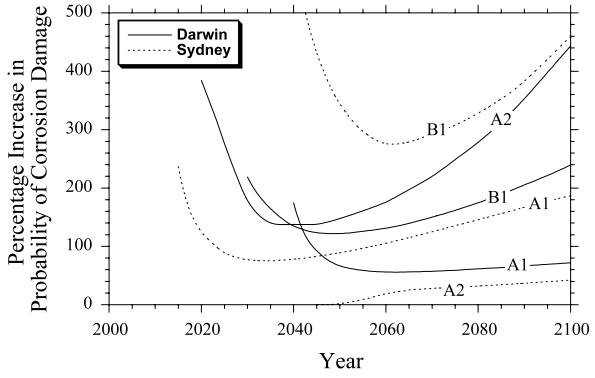

Fig. 7. Percentage increase in probability of carbonation-induced corrosion damage.

emission scenarios and larger diameter reinforcing bars, the proportional reduction of cross-sectional area reduces further.

7.3. Chlorides

Fig. 8 reviews the probabilities of corrosion initiation and corrosion damage for all emission scenarios, exposure classifications and locations. The durability design specifications are enhanced for severe environments, such as concrete structures in splash and tidal zones (exposure classifications (C and C2)), but the associated high concrete cover, increased concrete compressive strength and low w/c ratio is counter-balanced by the higher chloride exposures, resulting in probabilities of corrosion initiation and damage that reach 20%–40% (see Fig. 8). On the other hand, probabilities of corrosion initiation and damage are negligible for less severe exposure classifications B1, B2 and C1 even though durability design specifications are not as stringent. The corrosion rate for tidal and splash zones (C and C2) are very high at 6.035 $\mu A/cm^2$—hence once corrosion has initiated, the time to severe cracking (T_{sev}) is only several years. This means that the probability of corrosion damage is only slightly less than the probability of corrosion initiation.

It is evident from Fig. 8 that the corrosion initiation and damage risks are not influenced considerably by the emission scenario. For example, corrosion damage risks for the worst emission scenario (A1FI) are only 6%–15% higher than the reference (best) emission scenario. This shows that while predicted increases in temperature will increase chloride diffusion coefficient and corrosion rate, these increases will be relatively modest with relatively little influence on chloride-induced corrosion.

The additional corrosion loss of reinforcement for A1FI emission scenario (when compared to the reference mitigation scenario) and exposure C2 for Darwin and Sydney is 0.78 mm and 0.46 mm by 2100, respectively. These are the highest corrosion loss for any exposure. For a 16 mm diameter bar, this represents a 9.5% and 5.7% loss of cross-sectional area. The additional corrosion loss is lower for other exposure classifications or emission scenarios. These proportional reductions in cross-sectional area, which will reduce as bar diameter increases, will reduce structural safety, but this loss is not likely to be overly significant unless there is high localised pitting corrosion which can reduce structural reliability considerably (e.g., [47]). Nonetheless, this is an area for further research.

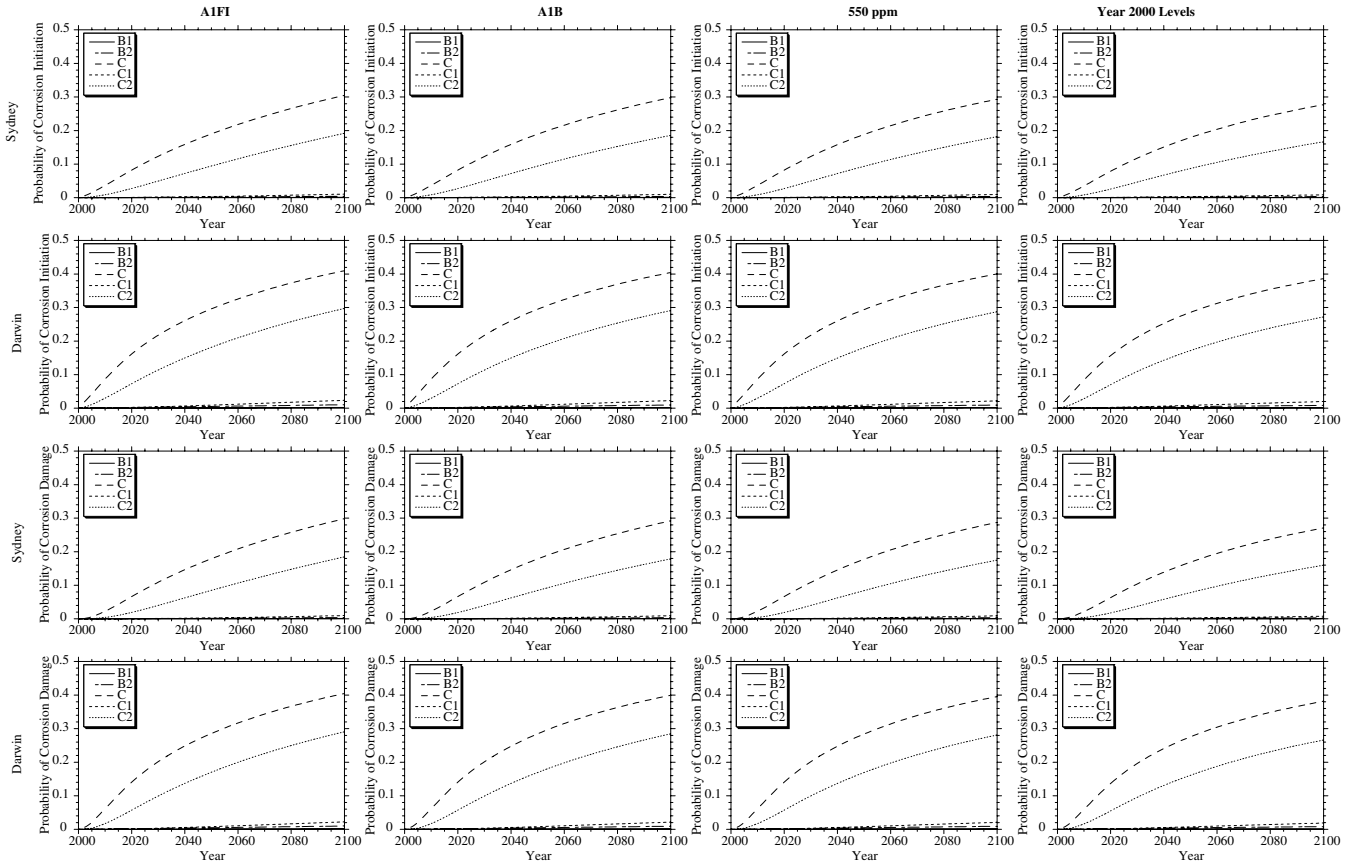

Fig. 8. Probabilities of chloride-induced corrosion initiation and corrosion damage, for Sydney and Darwin.

7.4. Practical applications and further research

Carbonation-induced corrosion is very low to negligible for concrete infrastructure located within 50 km of Sydney and Darwin, i.e., exposure classifications B1, B2 and C. However, corrosion damage risks for inland regions with arid or temperate climates (A1 and A2) can reach 20%–40% (see Fig. 6) and climate change can cause increases in damage risks by 40%–460% (see Fig. 7). Fortunately, a small proportion of Australia's infrastructure is located in these regions in Australia; however, these infrastructure may well merit appropriate and cost-effective adaptation measures.

Damage risks for chloride-induced corrosion are quite high because of the severe splash and tidal exposure of marine structures in water (exposure classifications C and C2). Concrete structures located away from the coast, or in the spray zone, have damage risks of less than 1%, and most are negligible. What is relevant to this discussion is that corrosion damage risks are high even for the reference mitigation scenario (year 2000 CO_2 levels held constant with time). So damage risks are already high today. Climate change will increase these risks by at most 6%–15%. These structures may merit appropriate and cost-effective adaptation measures, but the climatic effects on carbonation-induced corrosion seem more severe and a priority for adaptation measures.

The results presented are based on durability design specifications of AS3600-2009 [40], which relate to minimum concrete cover and concrete compressive strength only. It is important to note that, for a specific structure, accurate results in terms of climate change impact and damage risks can be obtained only by considering structural typology, structural detailing, structure orientation, and other structure specific information.

An economic assessment of adaptation measures including increased cover, increased concrete mix durability, galvanised or stainless steel reinforcement, and coatings is essential in order to better manage concrete infrastructure over the next 100 years. A preliminary economic assessment of increasing design cover has been undertaken (e.g., [10]), but there is much scope for further research.

8. Conclusions

A time-dependent reliability analysis has been conducted to assess the probabilities of corrosion initiation and corrosion damage for existing concrete infrastructure subject to change of climatic variables to 2100. The loss of reinforcement cross-section was also calculated. The atmospheric CO_2 concentration and local temperature and humidity changes with time over the next 100 years were projected for the Australian cities of Sydney and Darwin as these cities are representative of temperate and tropical climates, respectively. Temperature and humidity projections were based on nine General Circulation Models (GCMs) under A1B, A1FI and 550 ppm stabilisation CO_2 emission scenarios. The reference or 'best' case mitigation scenario where CO_2 levels are held constant at year 2000 levels was also considered. The probabilistic analysis included the uncertainty of CO_2 concentration, deterioration processes, material properties, dimensions, and predictive models. It was found that carbonation-induced damage risks can increase by over 400% by 2100 for inland arid or temperate climates in Australia. Damage risks for chloride-induced corrosion increase by no more than 15%. Corrosion loss of reinforcement amounted to no more than 9.5% for chloride-induced corrosion. The results were most sensitive to increases in atmospheric CO_2. Structures located in inland arid or temperate climates in Australia were most susceptible to climate change, and these structures may merit appropriate and cost-effective adaptation measures.

Acknowledgements

The paper is based on a part of the research in the project 'An Analysis of the Implications of Climate Change Impacts for Concrete Deterioration', co-funded by the Australian Government Department of Climate Change and Energy Efficiency and CSIRO Climate Adaptation National Research Flagship. The authors would like to express their appreciation to Jo Mummery, Catherine Farrell, Robert Davitt and Mark Eslake of the Department, Allen Kearns, Seona Meharg, Phillip Paevere and Greg Foliente of CSIRO, for their support during the research. The authors also appreciate the assistance of Michael Netherton and Xiaoli Deng from The University of Newcastle.

References

[1] Val D, Stewart MG, Melchers RE. Effect of reinforcement corrosion on reliability of highway bridges. Eng Struct 1998;20(11):1010–9.
[2] Stewart MG, Mullard JA. Spatial time-dependent reliability analysis of corrosion damage and the timing of first repair for RC structures. Eng Struct 2007;29(5):1457–64.
[3] Akiyama M, Frangopol DM, Yoshida I. Time-dependent reliability analysis of existing RC structures in a marine environment using hazard associated with airborne chlorides. Eng Struct 2010;32(11):3768–79.
[4] IPCC. Fourth assessment report of the intergovernmental panel in climate change. UK: Cambridge University Press; 2007.
[5] Stewart MG, Rosowsky DV. Structural safety and serviceability of concrete bridges subject to corrosion. J Struct Eng, ASCE 1998;4(4):146–55.
[6] Sudret B, Defaux G, Pendola M. Stochastic evaluation of the damage length in RC beams submitted to corrosion of reinforcing steel. Civ Eng Environ Syst 2007;24(2):165–78.
[7] Fib. Model code for service life design, fib. Lausanne: Bulletin 34; February 2006.
[8] Stewart MG, Teply B, Kralova H. The effect of temporal and spatial variability of ambient carbon dioxide concentrations on carbonation of RC structures. In: 9th international conference on durability of building materials and components. CSIRO. 2002. Paper 246 [CD-ROM].
[9] Peng J, Stewart MG. Carbonation-induced corrosion damage and structural safety for concrete under enhanced greenhouse conditions. Research report no. 270.11.2008. NSW (Australia): Centre for Infrastructure Performance and Reliability, The University of Newcastle; 2008.
[10] Stewart MG, Peng J. Life cycle cost assessment of climate change adaptation measures to minimise carbonation-induced corrosion risks. Int J Eng Under Uncertain Hazards Assess Mitigation 2010;2(1–2):35–46.
[11] Bastidas-Arteaga E, Chateauneuf A, Sanchez-Silva M, Bressolette Ph, Schoefs F. Infuence of weather and global warming in chloride ingress into concrete: a stochastic approach. Struct Safe 2010;32:238–49.
[12] El Hassan J, Bressolette P, Chateauneuf A, Tawil K. Reliability-based assessment of the effect of climatic conditions on the corrosion of RC structures subject to chloride ingress. Eng Struct 2010;32(7):3279–87.
[13] IPCC. In: Nakicenovic N, Swart R, editors. Emission scenarios. Special report of the intergovernmental panel on climate change. UK: Cambridge University Press; 2000.
[14] Wigley TML, Richels R, Edmonds JA. Economic and environmental choices in the stabilization of atmospheric CO_2 concentrations. Nature 1996;379:240–3.
[15] Wang X, Chen D, Ren Z. Assessment of climate change impact on residential building heating and cooling energy requirement in Australia. Build Environ 2010;45(5):1663–82.
[16] George K, Ziska LH, Bunce JA, Quebedeaux B. Elevated atmospheric CO_2 concentration and temperature across an urban–rural transect. Atmos Environ 2007;41:7654–65.
[17] Day TA, Gober P, Xiaong FS, Wentz E. Temporal patterns in near surface CO_2 concentrations over contrasting vegetation types in the pheonix metropolitan area. Agric For Meteorol 2002;110:229–45.
[18] DuraCrete. 1998. Modelling of degradation. DuraCrete—probabilistic performance based durability design of concrete structures. EU—brite EuRam III. Contract BRPR-CT95-0132. Project BE95-1347/R4-5. December 1998. p. 174.
[19] Yoon IS, Copuroglu O, Park KB. Effect of global climatic change on carbonation progress of concrete. Atmos Environ 2007;41:7274–85.
[20] DuraCrete. 2000. Probabilistic calculations. DuraCrete—probabilistic performance based durability design of concrete structures. EU—brite EuRam III. Contract BRPR-CT95-0132. Project BE95-1347/R12-13. May 2000. p. 41.
[21] Sanjuan MA, del Olmo C. Carbonation resistance of one industrial mortar used as a concrete coating. Build Environ 2001;36(8):949–53.
[22] de Larrard F. Concrete mixtures proportioning: a scientific approach. London: E & FN Spon; 1999.
[23] Baccay MA, Otsuki N, Nishida T, Maruyama S. Influence of cement type and temperature on the rate of corrosion of steel in concrete exposed to carbonation. Corrosion 2006;62(6):811–21.
[24] DuraCrete. 2000. Statistical quantification of the variables in the limit state functions. DuraCrete—probabilistic performance based durability design of concrete structures. EU—brite EuRam III. Contract BRPR-CT95-0132. Project BE95-1347/R9. January 2000. p. 130.
[25] Kada-Benameur H, Wirquin E, Duthoit B. Determination of apparent activation energy of concrete by isothermal calorimetry. Cem Concr Res 2000;30:301–5.
[26] Russell D, Basheer PAM, Rankin GIB, Long EA. Effect of relative humidity and air permeability on prediction of the rate of carbonation of concrete. Proc Inst Civ Eng 2001;146(3):319–26.
[27] Al-Khaiat H, Fattuhi N. Carbonation of concrete exposed to hot and arid climate. J Mater Civ Eng 2002;14(2):97–107.
[28] Bary B, Sellier A. Coupled-carbon dioxide–calcium transfer model for carbonation of concrete. Cem Concr Res 2004;34(7):1859–72.
[29] Raupach M. Models for the propagation phase of reinforcement corrosion—an overview. Mater Corros 2006;57(8):605–13.
[30] Enevoldsen JN, Hansson CM, Hope BB. The influence of internal relative humidity on the rate of corrosion of steel embedded in concrete and mortar. Cem Concr Res 1994;24(5):1372–82.
[31] Neville A. Chloride attack of reinforced concrete: an overview. Mater Struct 1995;28:63–70.
[32] Vu KAT, Stewart MG. Structural reliability of concrete bridges including improved chloride-induced corrosion models. Struct Safe 2000;22(4):313–33.
[33] Val D, Stewart MG. Reliability assessment of ageing reinforced concrete structures—current situation and future challenges. Struct Eng Internat 2009;19(2):211–9.
[34] Val D, Stewart MG. Life cycle cost analysis of reinforced concrete structures in marine environments. Struct Safe 2003;25(4):343–62.
[35] BS 6349-1:2000. Maritime structures. Part 1: code of practice for general criteria. British Standard.
[36] El Maaddawy T, Soudki KA. A model for prediction of time from corrosion initiation to corrosion cracking. Cem Concr Compos 2007;29(3):168–75.
[37] Mullard JA, Stewart MG. Corrosion-induced cover cracking: new test data and predictive models. ACI Struct J 2011;108(1):71–9.
[38] Stewart MG. Serviceability reliability analysis of reinforced concrete structures. J Struct Eng, ASCE 1996;122(7):794–803.
[39] Stewart MG. Spatial variability of pitting corrosion and its influence on structural fragility and reliability of RC beams in flexure. Struct Safe 2004;26(4):453–70.
[40] AS3600. Concrete structures. Sydney: Standards Australia; 2009.
[41] Pham L. Reliability analysis of reinforced concrete and composite column sections under concentric loads. Civ Eng Trans, IEAust 1985;CE27(1):68–72.
[42] McGee R. Modelling of durability performance of tasmanian bridges. Melchers RE, Stewart MG, editors. ICASP8 applications of statistics and probability in civil engineering, vol. 1. 1999. p. 297–306.
[43] Mirza SA, Hatzinikolas M, MacGregor JG. Statistical descriptions of strength of concrete. J Struct Div, ASCE 1979;105(ST6):1021–37.
[44] Val D, Stewart MG. Safety factors for assessment of existing structures. J Struct Eng, ASCE 2002;128(2):258–65.
[45] Strauss A, Frangopol DM, Kim S. Use of monitoring extreme data for the performance prediction of structures: Bayesian updating. Eng Struct 2008;30(12):3654–66.
[46] Deby F, Carcasses M, Sellier A. Toward a probabilistic design of reinforced concrete durability: application to a marine environment. Mater Struct 2009;42:1379–91.
[47] Stewart MG. Mechanical behaviour of pitting corrosion of flexural and shear reinforcement and its effect on structural reliability of corroding RC beams. Struct Safe 2009;31(1):19–30.